REPORT DOCUMENTATION PAGE

1. REPORT DATE (DD-MM-YYYY) 23-05-2007	2. REPORT TYPE Technical Paper	3. DATES COVERED (From - To)

4. TITLE AND SUBTITLE

Thermographic Characterization and Comparison of 200W and 600W Hall Thrusters (Preprint)

5a. CONTRACT NUMBER

5b. GRANT NUMBER

5c. PROGRAM ELEMENT NUMBER

6. AUTHOR(S)
Taylor S. Matlock (Jackson and Tull); William A. Hargus & C. William Larson (AFRL/PRSS)

5d. PROJECT NUMBER
23080535

5e. TASK NUMBER

5f. WORK UNIT NUMBER

7. PERFORMING ORGANIZATION NAME(S) AND ADDRESS(ES)

Air Force Research Laboratory (AFMC)
AFRL/PRSS
1 Ara Drive
Edwards AFB CA 93524-7013

8. PERFORMING ORGANIZATION REPORT NUMBER

AFRL-PR-ED-TP-2007-291

9. SPONSORING / MONITORING AGENCY NAME(S) AND ADDRESS(ES)

Air Force Research Laboratory (AFMC)
AFRL/PRS
5 Pollux Drive
Edwards AFB CA 93524-70448

10. SPONSOR/MONITOR'S ACRONYM(S)

11. SPONSOR/MONITOR'S NUMBER(S)
AFRL-PR-ED-TP-2007-291

12. DISTRIBUTION / AVAILABILITY STATEMENT

Approved for public release; distribution unlimited (07220A)

13. SUPPLEMENTARY NOTES
For presentation at the 43rd AIAA/ASME/SAE/ASEE Joint Propulsion Conference, Cincinnati, OH, 8-11 July 2007.

14. ABSTRACT

Thermal analysis of Hall thrusters is necessary for both performance optimization and spacecraft integration. The thermal characteristics of the thruster influence the lifetime, energy losses, and spacecraft integration. The lifetime of most Hall thrusters is limited by the erosion of the insulating materials within the discharge chamber, which may vary with temperature. Thruster thermal data are also indicative of thruster energy losses as well as the heating characteristics of spacecraft interface surfaces. The results of the thermographic imaging of two laboratory Hall thrusters, a 200W (BusekBHT-200-X3) and 600W (BusekBHT-600), are presented. Surface temperature profiles were obtained using an infrared camera (7-13μm), independently verified by thermocouples. Infrared imagery of thruster start-up, steady-state, and shut-down was recorded and used to approximate the transient heating behavior of each thruster. Variation of the nominal mass flow rate (resulting in proportional variation of the anode current and power level) between 85% to 115% resulted in proportional changes to the thruster surface temperatures.

15. SUBJECT TERMS

16. SECURITY CLASSIFICATION OF:			17. LIMITATION OF ABSTRACT	18. NUMBER OF PAGES	19a. NAME OF RESPONSIBLE PERSON Dr. William A. Hargus
a. REPORT Unclassified	b. ABSTRACT Unclassified	c. THIS PAGE Unclassified	SAR	22	19b. TELEPHONE NUMBER (include area code) N/A

Thermographic Characterization and Comparison of 200W and 600W Hall Thrusters (Preprint)

Taylor S. Matlock*

Jackson & Tull, Edwards AFB, CA, 93524

William A. Hargus Jr.† and C. William Larson‡

AFRL/PRSS, Edwards AFB, CA, 93524§

Thermal analysis of Hall thrusters is necessary for both performance optimization and spacecraft integration. The thermal characteristics of the thruster influence the lifetime, energy losses, and spacecraft integration. The lifetime of most Hall thrusters is limited by the erosion of the insulating materials within the discharge chamber, which may vary with temperature. Thruster thermal data are also indicative of thruster energy losses as well as the heating characteristics of spacecraft interface surfaces. The results of the thermographic imaging of two laboratory Hall thrusters, a 200 W (Busek BHT-200-X3) and 600 W (Busek BHT-600), are presented. Surface temperature profiles were obtained using an infrared camera (7-13 μm), independently verified by thermocouples. Infrared imagery of thruster start-up, steady-state, and shut-down was recorded and used to approximate the transient heating behavior of each thruster. Variation of the nominal mass flow rate (resulting in proportional variation of the anode current and power level) between 85% to 115% resulted in proportional changes to the thruster surface temperatures.

I. Introduction

The Hall thruster is a high specific impulse electric thruster, well suited for missions requiring continuous low thrust maneuvers using minimal propellant mass. Spacecraft integration, erosion of insulating materials (thruster lifetime), and low efficiencies at low power levels are some of the issues facing Hall thrusters. This study examines the temperature of various surfaces of a Hall thruster with a long wave infrared camera. IR cameras work by relating incoming electromagnetic radiation of a specified infrared spectral band to surface temperatures using calibration curves. The raw temperature reading provided by the camera assumes the examined surface radiates as a blackbody (emissivity of 1.0) through a vacuum (transmissivity of 1.0).

A combination of Kirchoff's law with the Stefan-Boltzmann equation yields Equation 1, which describes the general relationship between actual and measured temperature based on the optical properties of the object in question.[15] Here, T_{cam} refers to the blackbody temperature indicated by the camera, T_{obj} is the surface temperature we are attempting to extract, T_{refl} is the effective temperature of radiation incident on the surface, and T_{vp} is the temperature of the viewport in use.

$$T_{cam}^4 = \epsilon\tau_{vp}T_{obj}^4 + (1-\epsilon)\tau_{vp}T_{refl}^4 + (1-\tau_{vp})T_{vp}^4 \qquad (1)$$

Transmissivity, τ, and emissivity, ϵ, are dependent on material, wavelength and temperature. Emissivity is also a function of direction, surface roughness, oxide layers, and contaminants, among other factors, making the determination of emissivity from literature problematic.[15] The sputtering and deposition processes inherent to the experiment may also cause some time-dependent fluctuation in emissivity as well as viewport transmission.

---

*Engineer, Jackson & Tull, 1 ARA Rd Edwards AFB, CA, 93524, AIAA Member.
†Engineer, AFRL/PRSS, 1 ARA Rd Edwards AFB, CA, 93524, AIAA Senior Member.
‡Scientist, AFRL/PRSS, 1 ARA Rd Edwards AFB, CA, 93524, AIAA Senior Member.
§Distribution A: Approved for public release; distribution unlimited

American Institute of Aeronautics and Astronautics

The first term on the right hand side of Eqn. 1 is proportional to the radiant energy emitted by the object being measured due only to its surface temperature. The second term accounts for any energy emitted by surrounding objects that is reflected by the surface of interest, when treated as a greybody. The third term indicates thermal radiation from the viewport material itself. Equation 1 demonstrates that the raw camera reading will underestimate the actual temperature of a low emissivity surface, unless the effective temperature reflected by the surface exceeds the surface temperature. Difficulties in accurately quantifying the reflected temperature make obtaining reliable measurements from surfaces with emissivities less than 0.5, such as polished metals, both troublesome and complicated, introducing significant uncertainties.

Two Hall thrusters, nominally 200 W and 600 W, were fired at various viewing angles and power levels, in order to characterize thruster operation and IR camera utility for a range of conditions. Thruster temperatures have been historically measured by thermocouples, but the integration of thermocouples in the discharge chamber is experimentally obtrusive and difficult due to severe environmental conditions.[3,8,9,11] Thermal imaging of Hall thrusters and cathodes has become increasingly common thanks to advancements in IR camera technology, and has been employed under a variety of methods and assumptions.[2,4–6,12] This work looks to expand on the current literature by more thoroughly examining the transient properties of Hall thrusters using commercial software and minimally obtrusive thermocouple measurements. In the following section the experimental setup is described, followed by a detailed description of each test and its corresponding results. Finally, conclusions are drawn as to the thermal properties of the thrusters and the usefulness of the camera as a diagnostic.

II.   Experimental Setup

All testing was performed in Chamber 6 at the Air Force Research Laboratory Electric Propulsion Laboratory at Edwards AFB, CA. This chamber is constructed of nonmagnetic stainless steel with a 1.8 m diameter and 3.0 m length. Four single stage cryo-panels (APD single stage cold heads at 25 K) and one 50 cm two stage APD cryo-pump (<12 K) provide a measured pumping speed of 32,000 l/s on xenon. The chamber is roughed by an oil free Stokes mechanical pump and blower. Background pressure in the chamber, measured by an ionization gauge, reached a maximum of 1.3 mPa, corrected for xenon, during 600 W thruster operation. Graphite panels were installed on one side of the chamber as a precautionary measure to minimize sputtering of the stainless steel chamber walls.

Infrared images were obtained using a FLIR Systems Thermovision® A40M Infrared Camera. The A40M uses an uncooled microbolometer focal plane array detector which measures incoming radiation at wavelengths between 7.5 and 13 μm with a spatial resolution of 1.3 mrad. ThermaCAM[TM] Researcher 2.8 software controls the camera through an IEEE-1394 interface and converts camera signal to temperature values, at speeds up to 60 Hz. The Researcher software is also used to account for such object parameters as emissivity and transmissivity, using a proprietary algorithm. The uncertainty in raw camera temperature measurements is the greater of $\pm$ 2 % or $\pm$ 2°C, as quoted by the manufacturer.

A zinc selenide (ZnSe) viewport, with a viewing diameter of 1.94 in., was installed on Chamber 6. The viewport material was selected for its high transmission in the spectral range of the IR camera. A representative plot of ZnSe transmission versus wavelength is presented in Fig. 1.[1]

A Graseby Infrared Model 564 blackbody radiation source and Model IR-201 temperature controller were used to calibrate the IR camera and software for transmission through the viewport. Camera measurements were made for a range blackbody temperatures. Transmission values needed to match measurements through the viewport to measurements without the viewport are plotted in Fig. 2 with respect to the initial temperature measurements with the viewport. Two calibration tests were performed with the blackbody radiation source.

An inverse square-root relationship yields a close fit to the blackbody calibration data. Equation 2, found by regression analysis, is used to estimate a viewport transmission value for each raw temperature measurement. The temperature threshold at 40°C occurs because the camera does not have the precision to differentiate between source and ambient radiation at values approaching room temperature. The viewport transmission is assumed to equal 92 %, the highest measured transmission, for temperatures below 40°C. The threshold temperature was calculated using the first part of Eqn. 2 and a transmission of 92 %.

$$\tau_{vp} = \begin{cases} \frac{0.8}{\sqrt{T-32°C}} + 0.633, & T > 40°C \\ 0.92, & T \leq 40°C \end{cases} \tag{2}$$

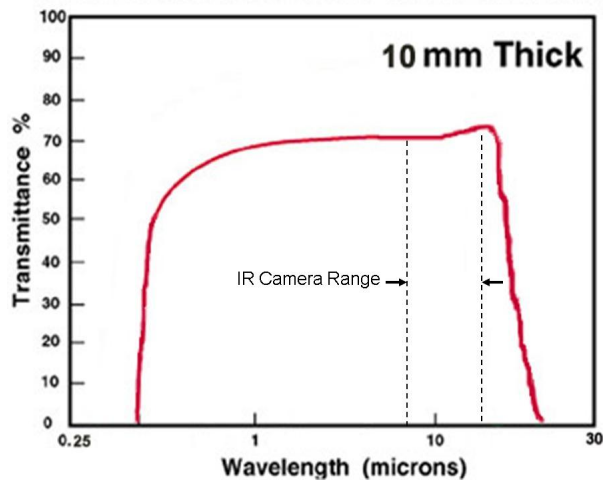American Institute of Aeronautics and Astronautics

Figure 1. Typical ZnSe transmission versus wavelength[1]

A. Hall Thrusters

The first Hall thruster examined is the Busek BHT-200-X3 200 W Laboratory Hall thruster, shown integrated inside AFRL Chamber 6 in Fig. 3. The nominal thruster operating conditions are shown in Table 1. A more detailed description of the thruster and the Chamber 6 support equipment is given elsewhere.[10]

The second thruster examined was a laboratory Busek BHT-600 600 W Hall thruster, allowing the comparison of two thrusters of differing power levels and geometry. The BHT-600, pictured in Figs. 5 and 6, runs at the nominal conditions given in Table 2 and was connected to the same power and xenon supplies used to operate the BHT-200-X3.[10]

Anode flow	840 μg/s (Xe)
Cathode flow	98 μg/s (Xe)
Anode potential	250 V
Anode current	0.85 A
Keeper current	0.5 A
Magnet current	1.0 A
Heater current	3.0 A

Table 1. BHT-200-X3 Nominal Operating Conditions[10]

The thrusters were mounted on a rotary stage which enabled the firing angle of the thruster to be varied during testing, to a 3 arcsecond resolution. The rotary stage was controlled using an IDC S6002 Dual-Axis MicroStepping Device through a National Instruments UMI-7764 interface connected to a Dell Dimension 8100 with LabView 7.1. The angle measurement convention used is shown in Fig. 4, with the axis of rotation running through the center of the thruster exit plane. The rotary stage was placed 71 cm from the ZnSe viewport along the viewport normal.
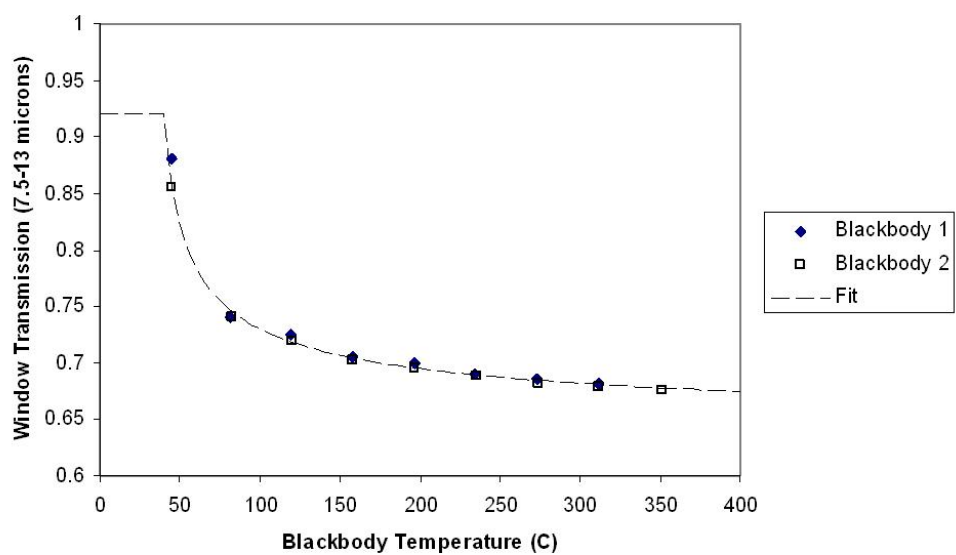
American Institute of Aeronautics and Astronautics

Figure 2. Viewport transmission between 7.5 and 13μm versus raw IR camera temperature with an emissivity of 1.0
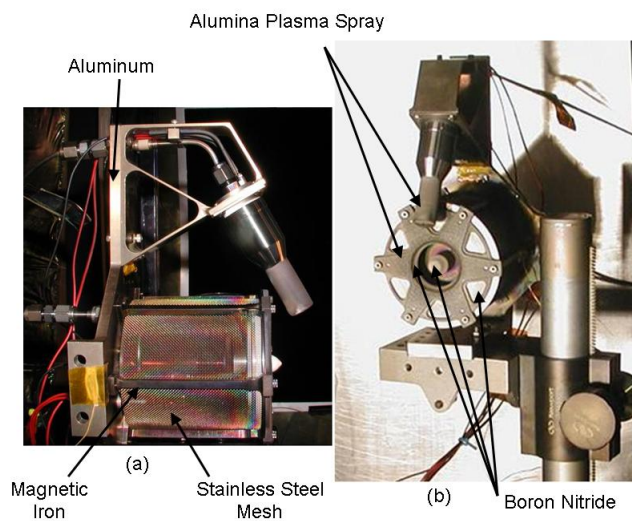
Figure 3. Busek BHT-200-X3 Hall thruster installed on rotary stage (a) profile (b) face

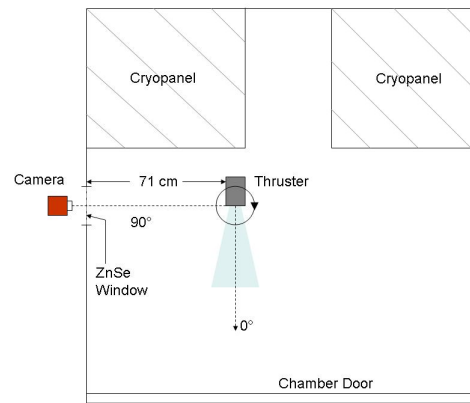American Institute of Aeronautics and Astronautics

Figure 4. Schematic of experimental apparatus and thruster firing angle convention
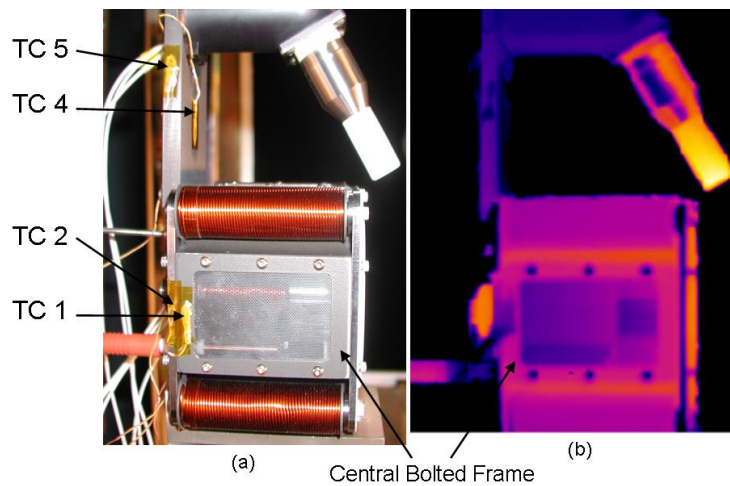

Figure 5. Busek BHT-600 Hall thruster installed on rotary stage (a) showing TC's (b) IR, firing at 0°
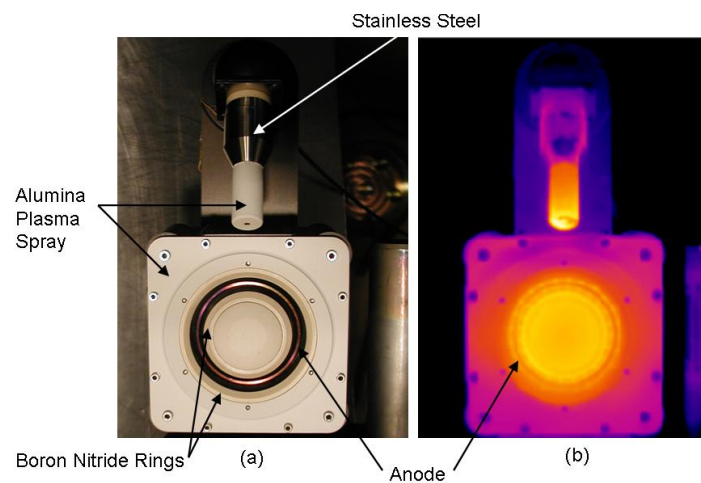

Figure 6. Busek BHT-600 Hall thruster installed on rotary stage (a) showing materials (b) IR, firing at 90°

American Institute of Aeronautics and Astronautics

Anode flow	2.5 mg/s (Xe)
Cathode flow	0.15 mg/s (Xe)
Anode potential	300 V
Anode current	2 A
Keeper current	0.5 A
Magnet current	1.75 A
Heater current	3.0 A

Table 2. BHT-600 Nominal Operating Conditions[10]

Type K thermocouples were used to validate camera temperature measurements. Five thermocouples were installed inside Chamber 6 and run through feedthroughs on the chamber wall to a National Instruments FP-TC-120 8 Channel Thermocouple Input. The thermocouple input was connected to a PC using a National Instruments FP-1601 10/100 Mbps Ethernet Network Interface. Four of the thermocouples were attached to the lower power thruster at the locations shown in Fig. 7. TC 5, not pictured in Fig. 7, was attached to the thruster in the same position as TC 2 on the side facing the camera at 0°. The third thermocouple was attached to the chamber wall beneath the ZnSe viewport, as shown in Fig. 8. All thermocouples, except TC 2, were attached using both Kapton tape and epoxy. TC 2 was attached using only Kapton tape in order to set a baseline for comparison with the epoxy attachment method. It was determined, after testing of the 200 W thruster, that Kapton tape was sufficiently adhesive during thruster operation, and that epoxy only added extraneous thermal mass.

All thermocouples on the 600 W thruster were attached using only Kapton tape, to the locations shown in Fig. 5. The thermocouple on the chamber wall was removed, then reattached to its original location without epoxy. Prior to attachment, proper operation of the thermocouple system was validated using an ice bath, and a standard uncertainty assumed of ± 0.75 % or ± 2.2°C.
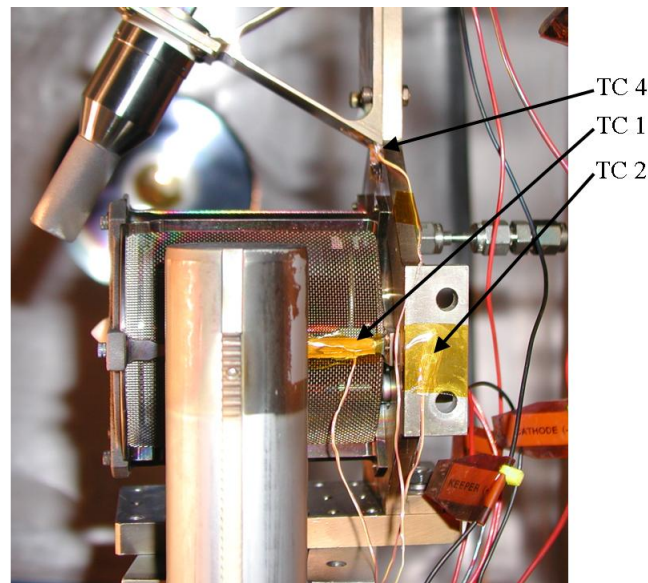

Figure 7. Busek BHT-200-X3 Hall thruster installed on rotary stage showing TC's, at 0°. TC 3 and TC 5 locations not visible

The region in and around the discharge chamber is one of the main areas of interest for diagnosing thruster operation. The discharge chamber of both thrusters examined here is insulated with boron nitride (BN). The effective emissivity of BN was examined by impregnating a flat sample with two type K thermocouples, then heating the sample and determining the emissivity input required to match IR camera output with TC measurements. Separate tests, using alternatively a hot plate and an oven to heat the Boron Nitride sample,

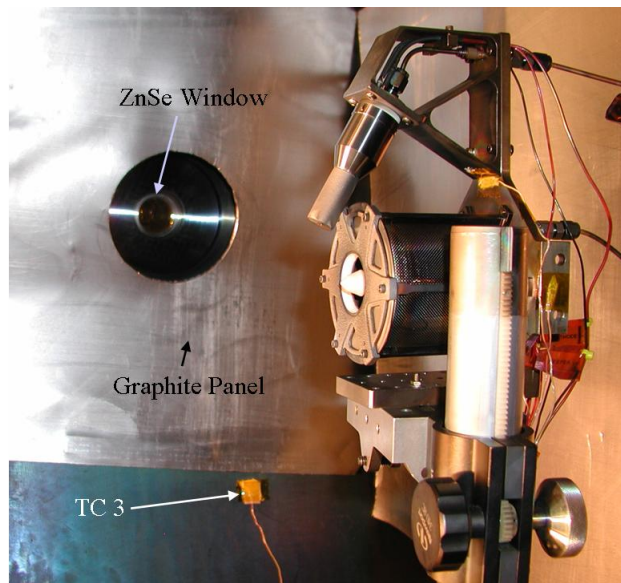American Institute of Aeronautics and Astronautics

Figure 8. Inside wall of AFRL Chamber 6 with BHT-200-X3 mounted on test apparatus

yielded similar results also displayed in Fig. 9.

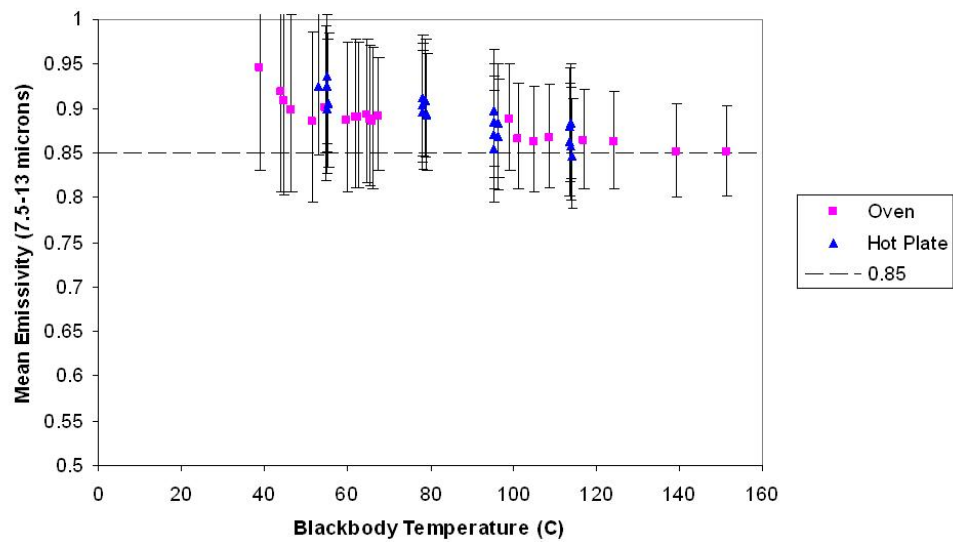Figure 9. Calculated Boron Nitride emissivity versus blackbody temperature indicated by IR camera

American Institute of Aeronautics and Astronautics

The results presented in Fig. 9 show that the blackbody assumption can be applied reasonably well to BN at low temperatures. Calculated emissivity appears to level out slightly at a value of 0.85, as the sample approaches the temperatures expected during thruster operation. All BN surfaces inside of the discharge chamber are treated as blackbodies in this work because the geometry precludes the practical extrication of emitted radiation from reflected. Boron Nitride surfaces outside of the discharge chamber are approximated with an emissivity of 0.85, compared to BN emissivities of 0.8 and 0.75 assumed by Roche et al. and Zhang et al., respectively.[7, 16] Uncertainty of the calculated emissivity was estimated by combining the errors in camera and thermocouple measurements.
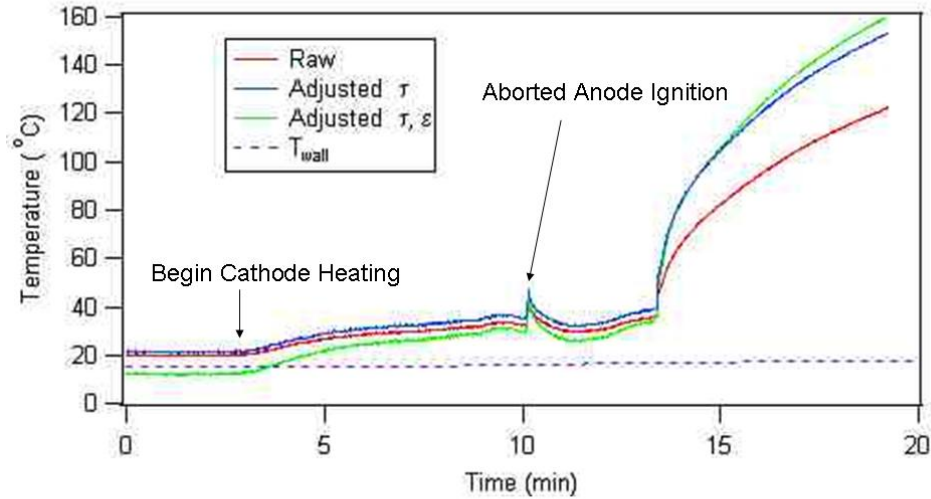

Figure 10. 600 W Thruster Inner Insulator Ring Temperature versus Time as seen from 90° with adjustments for measured viewport transmission and boron nitride emissivity

Raw camera data were applied to Equation 2 to correct for transmission, at the end of the experiment. Afterwards, any necessary emissivity alterations were applied in order to preserve the congruity between camera and thermocouple measurements, with TC 3 readings input as T_{refl}. The results following each stage of adjustment are presented, as an example, in Figure 10.

III.   Experimental Results

The aperture at the exit of the cathode is treated as a blackbody emitting the temperature internal to the cathode tip. Since the aperture is not visible at 0°, and there is no experimentally determined emissivity for the plasma spray alumina on the cathode surface, an estimate of the effective emissivity was necessary. It was found that an emissivity of 0.85 at the cathode tip provided the most congruity between the temperature measurements made at 0° and those made of the aperture at 90°.

A.   200 W Thruster

Emissivity estimates were made for several surfaces on the 200 W thruster by comparing camera with thermocouple measurements. As noted previously, TC 2 provided the only reliable thermocouple data for the 200 W thruster. In order to estimate an emissivity for the central magnetic iron strut, it is assumed that the temperature at the TC 1 location is closely approximated by TC 2, as the system approaches steady state conditions. The best fit of camera to thermocouple data is obtained with an emissivity of 0.11 for aluminum and 0.20 for iron.

The cathode for the 200 W thruster was conditioned for 90 minutes at nominal Xe flow, before firing for the first time. After conditioning, the cathode was ignited, then the anode was run at nominal conditions for 3.5 hours at a 0° angle. The anode power decayed from 202 W at start-up to 178 W in about 50 minutes, before leveling off. IR camera measurements during cathode ignition, anode ignition, nominal firing and

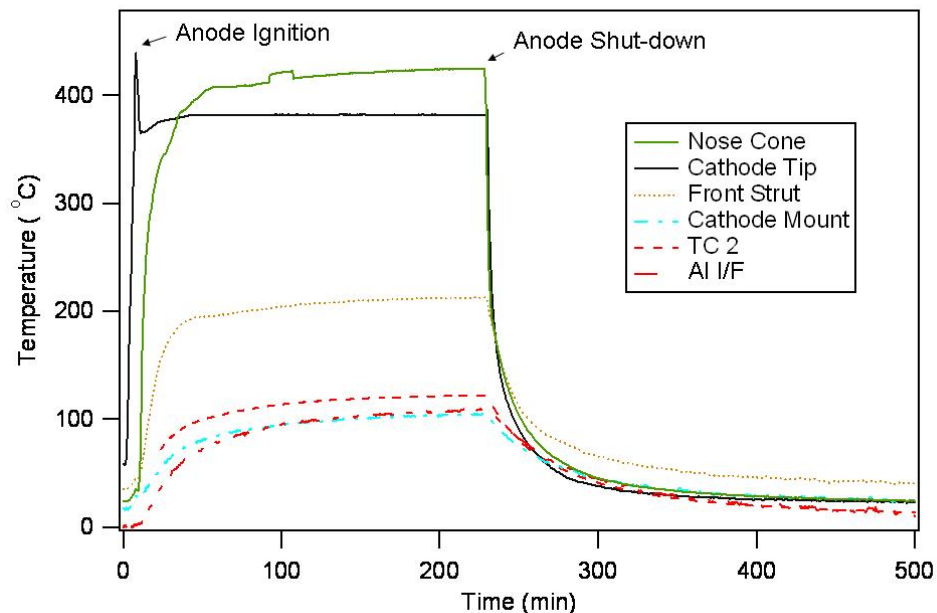shut-down are shown in Fig. 11, adjusted for emissivity and viewport transmission.

Figure 11. 200 W Thruster Temperatures versus Time for a 3.5 hour nominal burn, as seen from a 0° firing angle. Greybody emissivity is assumed.

The *Front Strut* measurements presented were taken at the point on the central iron strut closest to the thruster exit. The *Aluminum Interface* curve was measured from a point just above TC 5. The *Cathode Mount* refers to a point on the aluminum profile, unilateral with TC 4. The disparity between camera measurements on the bolted aluminum interface and TC 2 measurements are most likely due to an overestimation of the reflected temperature. The short jump in nose cone temperature observed at around 100 minutes is notable in that it is not mirrored by any other measurements at the time.

No cathode conditioning was required for the next 200 W thruster firing, which took place after 15 hours of cooling, resulting in cold starting conditions (Thruster ∼8°C). The thruster was fired for approximately 30 minutes. The camera measurements during pre-start, cathode ignition and the 30 minute burn are displayed in Fig. 12 along with TC 2 data. Once again the nose cone exhibits a sudden change in temperature not seen anywhere else on the thruster. Also of note is the reoccurance of a precipitous drop in cathode temperature accompanying ignition.

After the 30 minute nominal burn, the thruster was rotated to 90°, and the thruster power removed. The first 10 minutes of cooling can be seen in Fig. 13. The thruster was allowed to cool for 70 minutes before preparation of the next firing. After 70 minutes, most surfaces had cooled to about 30°C. During the short period between anode shut-down and cathode shut-down the cathode experiences a quick rise in temperature, visible in Figs. 13 and 14, corollary to the quick drop seen during start-up.

After cool-down, the thruster was re-ignited with an anode flow rate of 686 $\mu g/s$ of Xenon, resulting in an average anode power of 143 W. The thruster fired for approximately 3.5 hours before the anode flow rate was increased to 980 $\mu g/s$, corresponding to an anode power of 214 W. Surface temperatures measured at a 0° angle during hot start and mass flow rate variation are presented in Fig. 15.

The thruster was rotated to 90° and shut down after about 2.5 hours of firing at 214 W. The first 10 minutes of cool-down are displayed in Fig. 16. All surfaces are within 1°C of 25°C, as measured by the camera, four hours after the anode is turned off.

As expected, increasing the propellant mass flow rate, and hence the anode power, resulted in a marked rise in temperature. The increase of temperature with power has been predicted and verified experimentally with thermocouples on other Hall thruster models.[3,7] Steady state temperatures (2.5 hours) at each anode power are shown in Fig. 17. All surfaces, except the aluminum interface where TC 2 is located, show a waning increase in temperature with power.
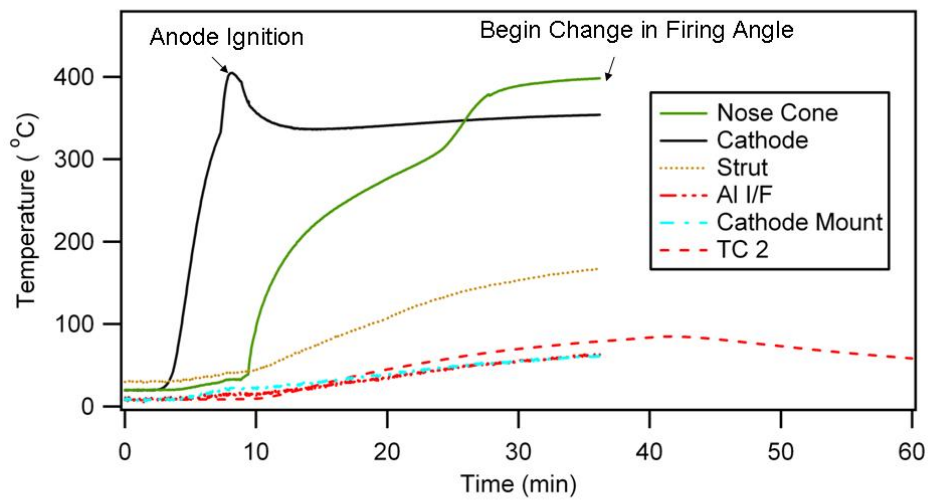
Figure 12. 200 W Thruster Temperatures versus Time for a 30 minute nominal burn from cold start, as seen from a 0° firing angle. Greybody emissivity is assumed.
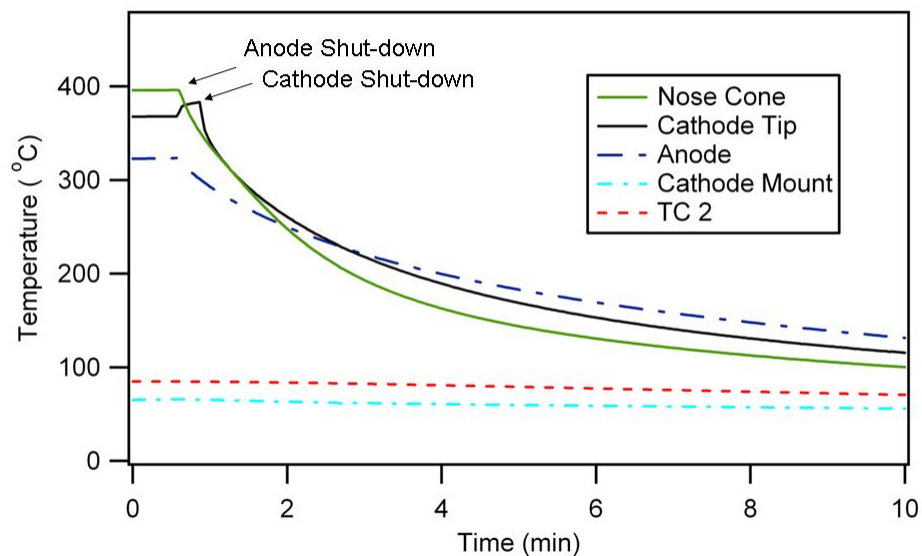

Figure 13. 200 W Thruster Temperatures versus Time for cool down after 30 minute nominal burn, as seen from 90°. Greybody emissivity is assumed.

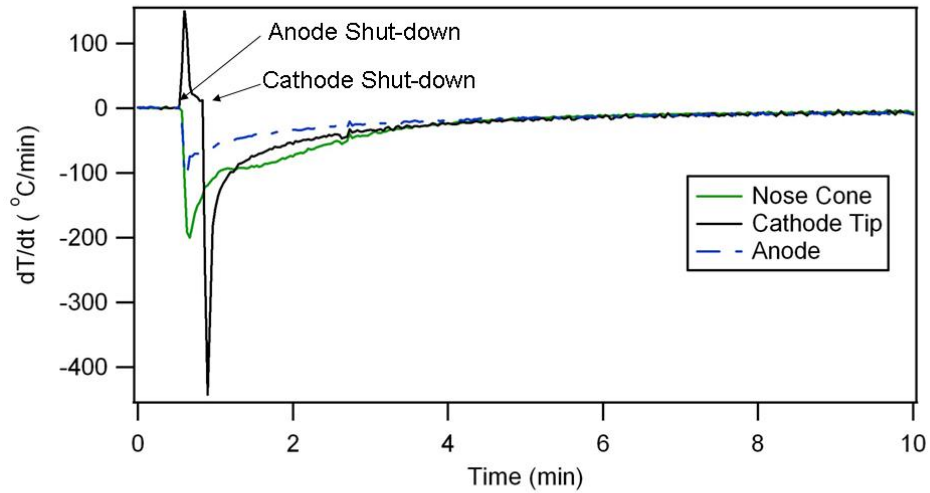American Institute of Aeronautics and Astronautics

Figure 14. 200 W Thruster Cooling Rate versus Time after 30 minute nominal burn, as seen from 90°. Greybody emissivity is assumed.

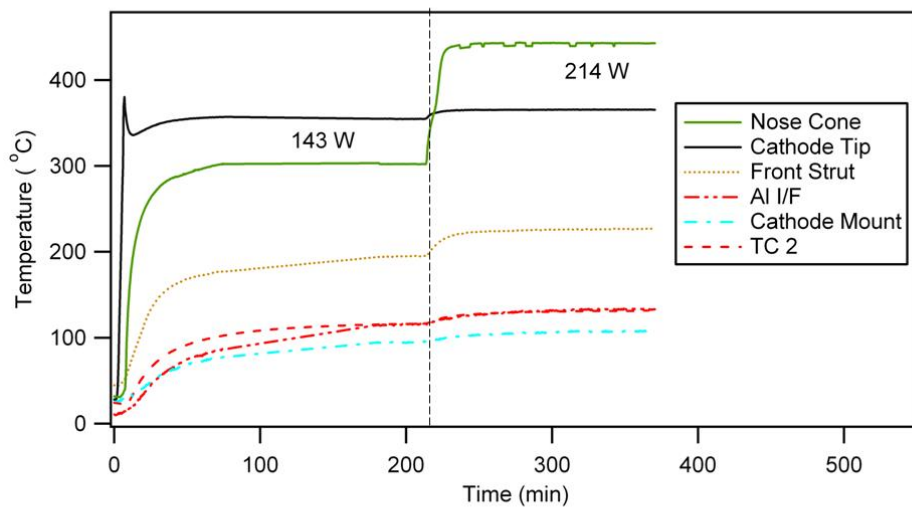**Figure 15. 200 W Thruster Temperatures versus Time as seen from 0° with varying anode mass flow rates. Greybody emissivity is assumed.**

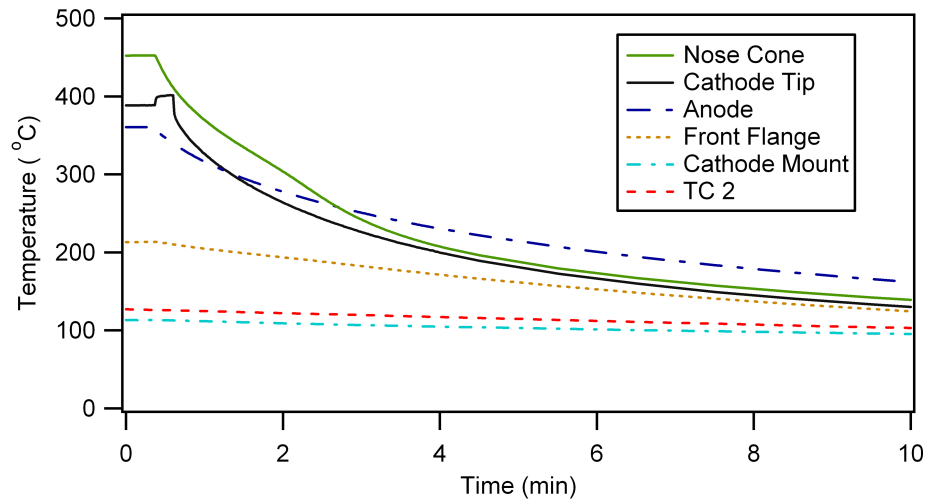American Institute of Aeronautics and Astronautics

Figure 16. 200 W Thruster Temperatures versus Time after off-nominal firing, as seen from a 90° firing angle. Greybody emissivity is assumed.
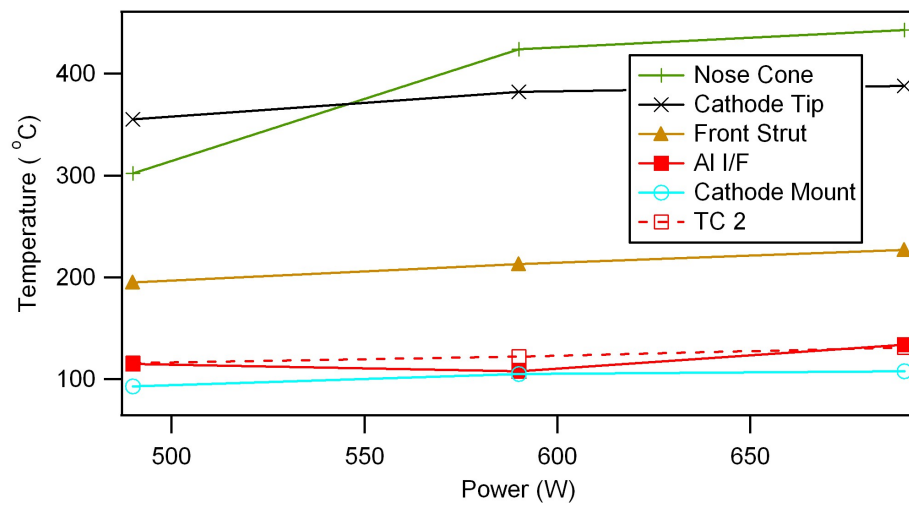

Figure 17. 200 W Thruster Temperatures versus Anode Power. Greybody emissivity is assumed.

B.   600 W Thruster

Thermocouple data were more abundant for the 600 W thruster, with only the occasional malfunction of TC 2 and TC 5. Thermocouple malfunction during 200 W testing was due simply to poor thermal connection, whereas the 600 W thermocouples experienced extreme anomalies due to electrical interference. All thermocouple malfunctions on the 600 W occurred while the anode was powered and the thruster firing at angles of 45° or less. Camera measurements, made at a 0° angle, were found to closely match the working thermocouples when assuming blackbody radiation. The blackbody assumption was therefore adopted on all surfaces without an experimentally determined emissivity. Figure 22 succinctly displays the differences in thermocouple and camera measurements at steady state, when blackbody emission is assumed. The consistent overestimation of thermocouple temperature by camera measurements, typically by about 5%, may be due to systematic error in the thermocouple setup or underestimated transmission by Eqn. 2.

The 600 W thruster cathode required several hours of conditioning before ignition could be accomplished. Surface temperatures during the final stages of cathode bake-out and a 3.5 hour burn at nominal conditions (590 W measured at the anode) are shown in Fig. 18. During the nominal burn, the thruster was rotated from 0° to 15° for 2 of every 20 minutes, in order to obtain temperature measurements on the thruster face.
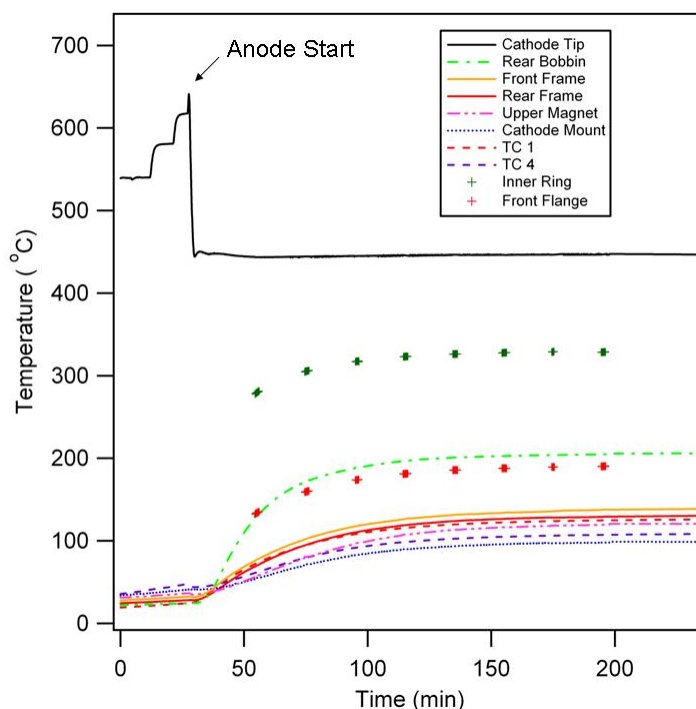

Figure 18.   600 W Thruster Temperatures versus Time as seen from 0°. Emissivity of 0.85 for the cathode and insulator ring. Emissivity is 1.0 for all other surfaces.

Rear Bobbin refers to the upstream extrusion of the central magnetic pole piece, shown, along with the *Upper Magnet*, in Figure 28. The *Rear Frame* measurement is taken on a point adjacent to TC 1, labeled in Fig. 5, opposite the *Front Frame*. Measurements on the *Inner Ring* indicate the maximum temperature viewed on the smaller BN piece, with *Front Flange* curves relaying the average temperature on the front plasma spray alumina surface.

The cathode tip exhibits several plateaus prior to anode ignition, each accompanying a rise in applied heater current. Near steady state the upper magnet emits a blackbody temperature of 120°C, while the rounded surface behind it emits at 155°C. The stainless steel cathode cover emits at a peak blackbody temperature of 200°C, which is likely much lower than the actual temperature, considering the low emissivity typical of shiny metal surfaces. Radiation from the central stainless steel mesh area reveals blackbody temperatures between 95°C and 130°C.

The 3.5 hour heating curve for the 600 W thruster is similar in shape to the 3.5 hour curve for the 200

American Institute of Aeronautics and Astronautics

W thruster, shown in Fig. 11. Rear surfaces on both thrusters reach about 100°C and the face plates level off near 200°C. The main difference appears on the hottest thruster surfaces. The inner ring of insulation on the 600 W is around 100°C cooler than the nose cone on the 200 W, while the cathode tip is nearly 70°C hotter. The difference in cathode temperature may be indicative of cathode age along with thruster power.[14]

The thruster was rotated to 90° at the end of the 3.5 hour burn to view steady state conditions on the entire thruster face. Azimuthal asymmetry in the temperatures on the insulating BN rings was observed, with temperature differences reaching 15°C. The 90° images show the predominance of symmetrically distributed spots of high temperature, adjacent to the anode. The spots, assumed to be the anode flow injectors, are presented graphically in Figures 19 & 20. According to camera measurements, the injector is emitting at a blackbody temperature of about 277°C, approximately 15°C hotter than the adjacent surface.
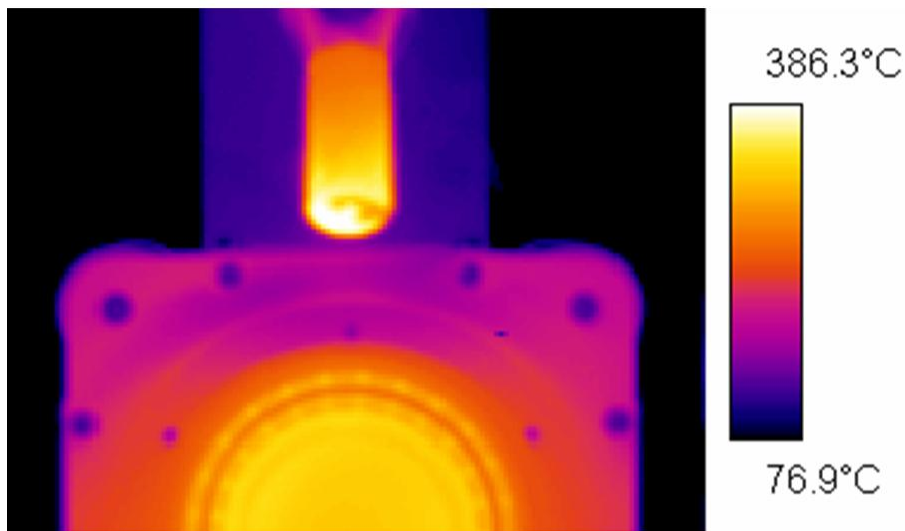

Figure 19. 600 W Thruster Face Temperature Distribution as seen from 90° assuming blackbody emission

A 30 minute nominal burn from cold start (Thruster ∼8°C) and a 70 minute cool down are shown in Figure 21. All surfaces on the 600 W, except the cathode, were slightly colder after the 30 minute burn than comparable surfaces on the 200 W. A steep jump in cathode temperature after anode shut down is not seen after the short duration burn.

After adequate time for thruster temperatures to approach ambient (∼70 minutes), the thruster was restarted with an anode mass flow rate of 2.12 mg/s, resulting in an average anode power of 490 W. Within 3 hours, the thruster temperatures had leveled off, and the mass flow rate was increased to 2.87 mg/s, sending 690 W to the anode. The clear increase in temperature accompanying the mass flow rate jump shown in Figure 21, is also evident in the surface temperature versus anode power plot in Figure 22.

The relationship between temperature and anode power is more consistent from surface to surface on the 600 W than the 200 W. Only the cathode mount displayed an increasing rate of temperature change with power, likely a product of errors in measurement. Every other surface exhibits a temperature-power curve that is actually closer to logarithmic than linear, with a slope that tends to decrease with the object temperature. The cathode temperature is shown as only weakly dependent on anode power, with all differences lying close to the uncertainty of the camera.

The cooling of thruster surfaces after the 5 hour, variable power, burn is shown in Fig. 23. In the time between anode shut-down and cathode shut-down, the cathode temperature is decreasing at a lower rate than it does after all power is removed. The 600 W is similar to the 200 W in that it takes about 5 hours for
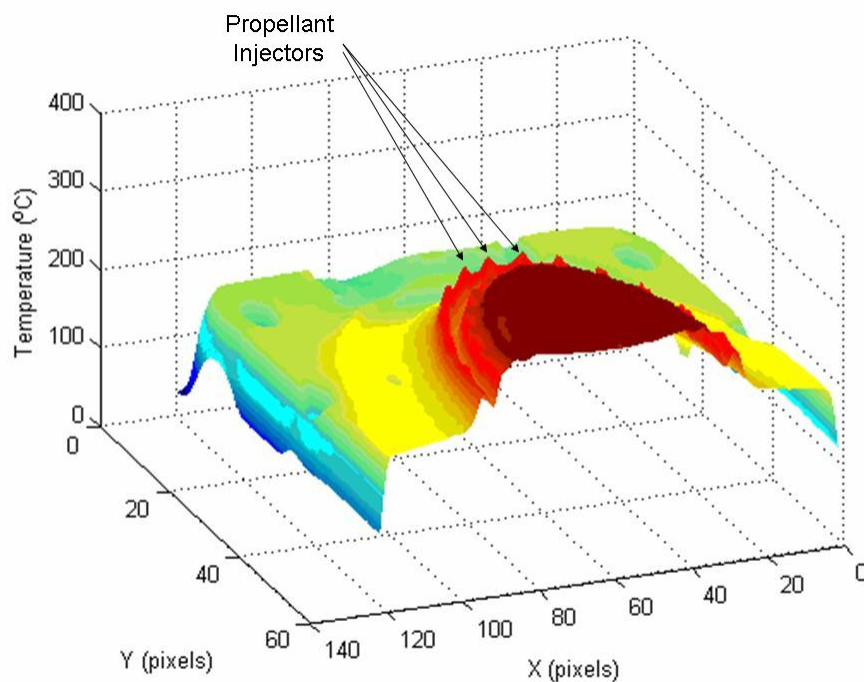
American Institute of Aeronautics and Astronautics

Figure 20. 3-D 600 W Thruster Face Temperature Distribution as seen from 90° assuming blackbody emission

surfaces to thermally equilibrate after shut-down. Figure 23 also emphasizes the deficiency of the camera, as compared to thermocouples, when surface temperatures approach ambient.

The 600 W was fired from a cold start at 90° in order to view the start-up characteristics of the thruster face. After 6 minutes the thruster was rotated to 60°, then 45° and 30° in 5 minute intervals. The thruster fired for another 85 minutes at a 30° angle before cool down, all of which is displayed in Fig. 24. Discrete drops in temperature are seen during thruster heating in Fig. 24, accompanying changes in firing angle, which are likely due to the unaccounted for directional variance of emissivity. Measurements from TC 3 show the chamber wall reaching 50°C as the thruster fires towards the thermocouple, then falling back to 20°C as the thruster turns to off-normal angles.

Identical burns were performed at two different directions to further examine the effects of thruster angle on camera measurements. Two 30 minute cold start burns were performed separately at 45° and 60°, displayed in Figs. 25 and 26 respectively. Camera measurements were slightly higher when performed at 60°, on all surfaces but the inner ring. The 45° angle exposes sections of the inner ring deeper into the discharge chamber, as illustrated in Fig. 27, where it appears hotter.
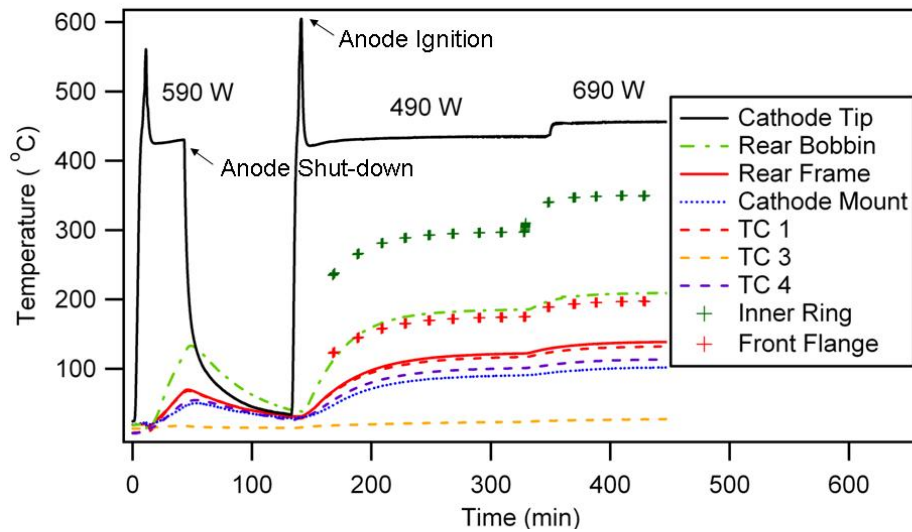
American Institute of Aeronautics and Astronautics

Figure 21. 600 W Thruster Temperatures versus Time as seen from 0° with varying anode mass flow rate. Emissivity of 0.85 for the cathode and insulator ring. Emissivity is 1.0 for all other surfaces.
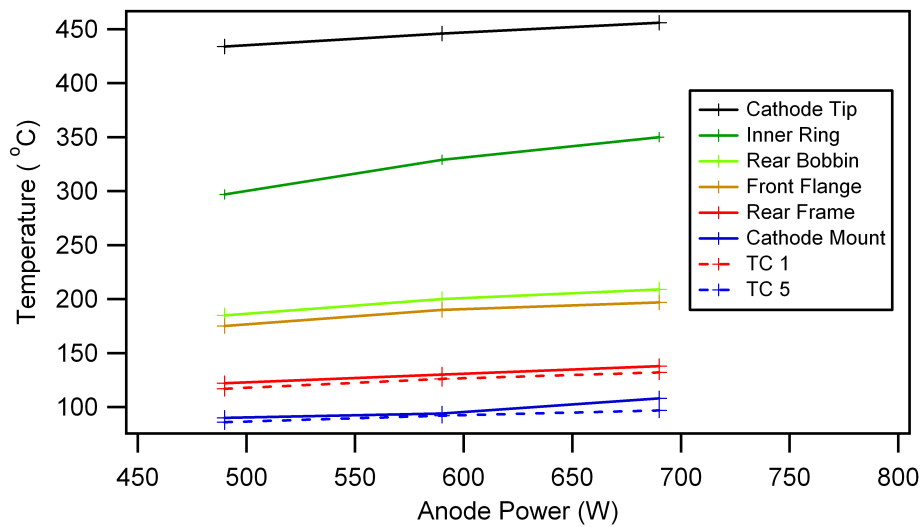

Figure 22. 600 W Thruster Temperatures versus Anode Power. Emissivity of 0.85 for the cathode and insulator ring. Emissivity is 1.0 for all other surfaces.
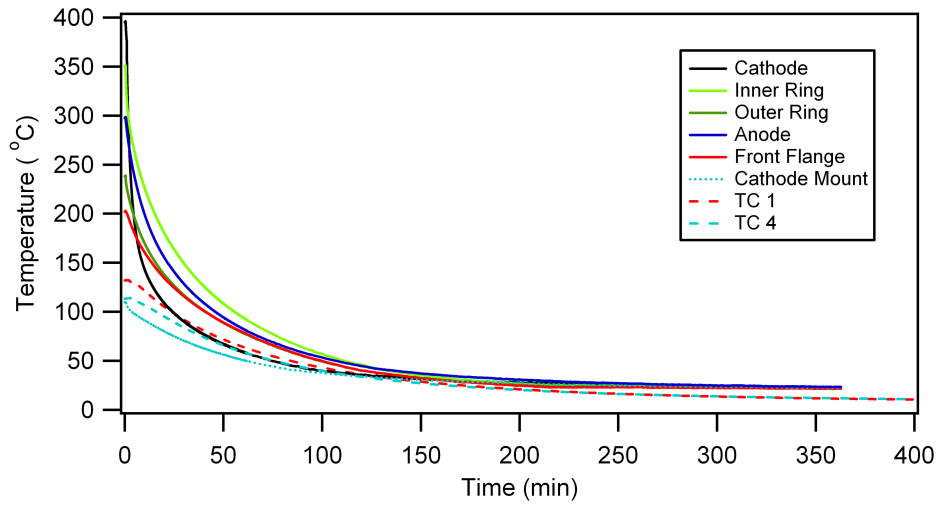
Figure 23. 600 W Thruster cool-down temperatures versus time as seen from 90° after 690 W operation
. Emissivity of 0.85 for the cathode and insulator rings. Emissivity is 1.0 for all other surfaces.
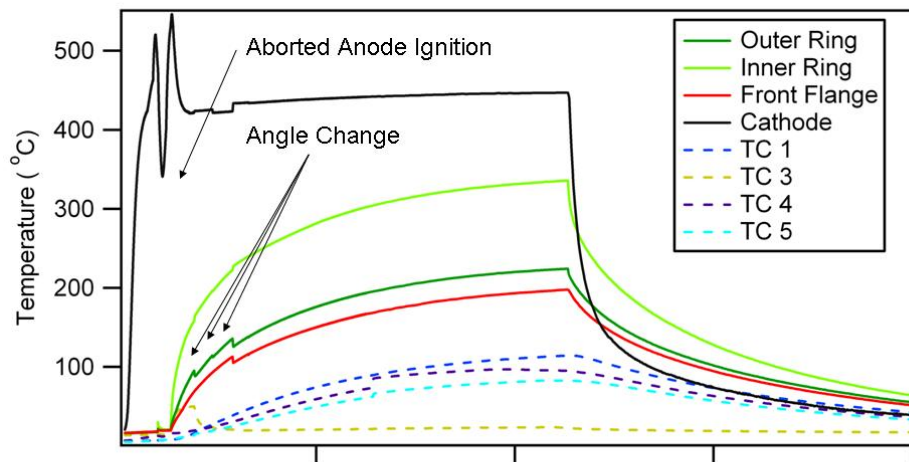

Figure 24. 600 W Thruster Temperatures versus Time as seen from varying angles. Emissivity of 0.85 for the cathode and insulator rings. Emissivity is 1.0 for all other surfaces.
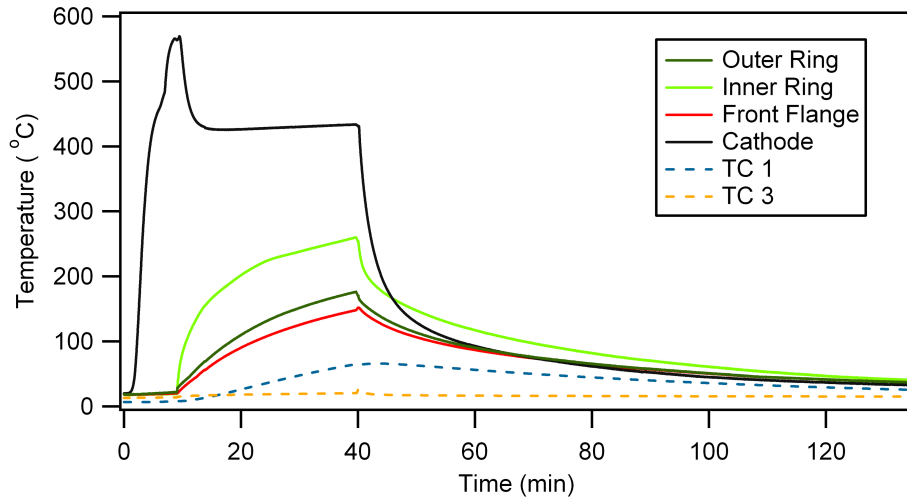
Figure 25. 600 W Thruster Temperatures versus Time as seen from 45°. Emissivity of 0.85 for the cathode and insulator rings. Emissivity is 1.0 for all other surfaces.
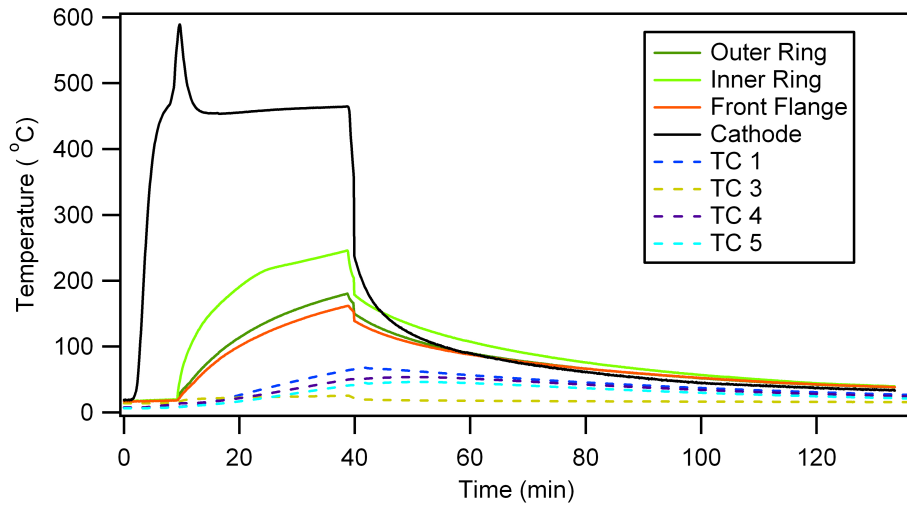

Figure 26. 600 W Thruster Temperatures versus Time as seen from 60°. Emissivity of 0.85 for the cathode and insulator rings. Emissivity is 1.0 for all other surfaces.
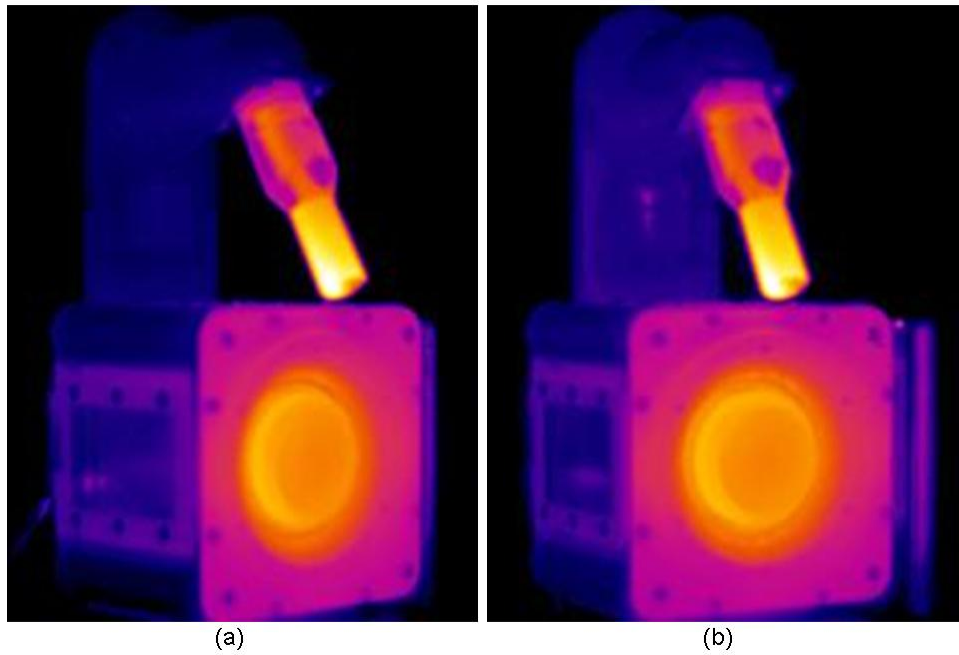
American Institute of Aeronautics and Astronautics

Figure 27. 600 W Thruster at (a) 45° (b) 60° angle
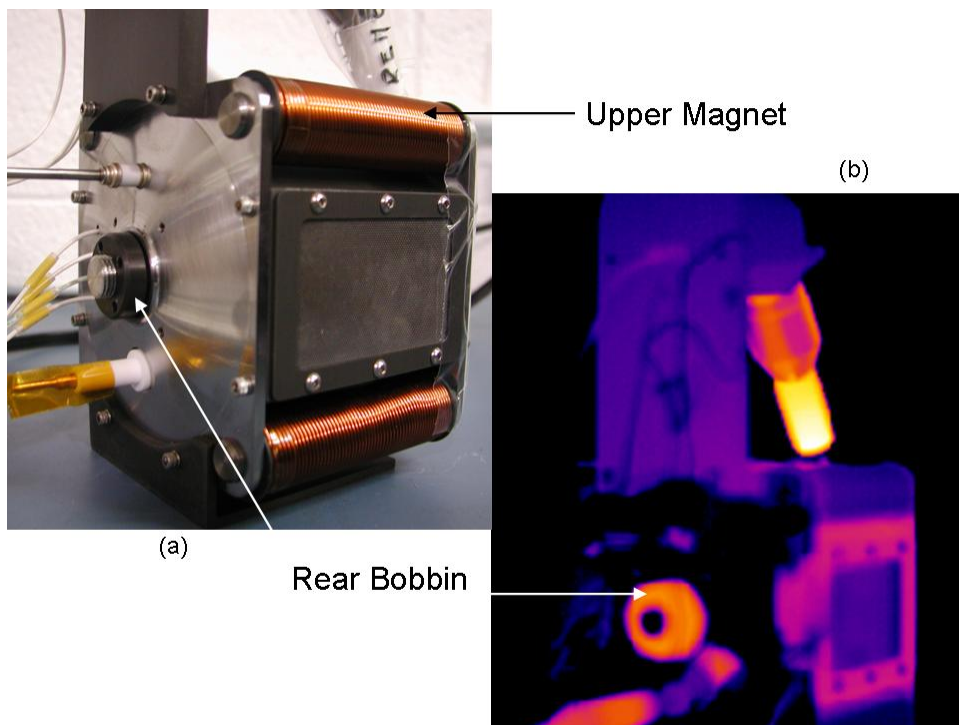
Figure 28. 600 W Thruster (a) Pre-installation (b) Cooling at a -60° angle

American Institute of Aeronautics and Astronautics

IV.   Conclusions

Thermographic imaging was conducted in an attempt to thermally characterize two Hall thrusters for a range of power levels and sizes, and to assess the applicability of the infrared camera as a thruster diagnostic. The camera was most effective as a tool for qualitative inspection. Relative infrared radiation from thruster components was displayed at angles varying from 0-90°. As long as incident radiation is less than emitted, the camera can provide a lower bound for the temperature of any surface. With some knowledge of the radiative properties of the system, an upper bound can be estimated as well, typically yielding a reasonable confidence interval.

The 200 W thruster was difficult to diagnose, due to the lack of thermocouple data and the low emissivity of most surfaces. The general heating trends measured agreed with expectations, based on other sources and the subsequent 600 W data.[3, 7–9] Anomalous heating was observed on the nose cone of the 200 W model, which may be the result of a change in the dominant heat transfer mode or possibly the erosion of contaminants. No significant changes in anode current or potential were measured during testing to match the anomalies, but it is possible that sputterants from the chamber wall and graphite paneling may have deposited in the discharge chamber, to be subsequently eroded off. It is also possible that as the temperature of the central solenoid increased, thereby increasing its resistance, conduction from the nose cone to the central pole piece attenuated and radiation became the primary mode of heat transfer.

A study by Raneev et al, has shown that the sputtering coefficient of Borosil (BN-SiO$_2$) doubling when the surface temperature was raised from 450°C to 590°C.[13] The temperatures measured on the center piece of the 200 W thruster approach the region where a high sensitivity of sputtering to temperature was shown, as illustrated in Fig 29. If BN exhibits a similar sputtering dependence on temperature, an increased thermal conductance from the center piece of small Hall thruster's, like the BHT-200, may have a dramatic effect on thruster lifetime.
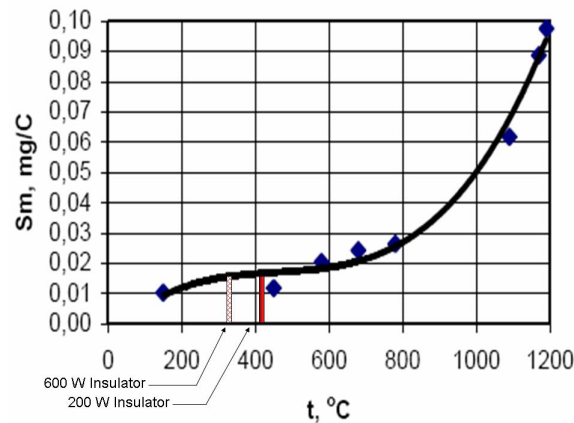

Figure 29. Borosil sputtering coefficient dependence on temperature (Xe^+, E_i=300 eV). Inner insulator temperatures shown for two Hall thrusters.[13]

A decreasing dependence of surface temperature with discharge current was shown on the inner chamber insulation of both thrusters. A 30% drop in temperature occured on the 200 W when the mass flow rate was less than nominal, with only a 4.5% increase at higher flow. This indicates that a small decrease in mass flow rate might be used effectively to cool a small thruster out of a high erosion regime. Conversely, the thruster may be throttled by increasing mass flow without incurring a substantial heating penalty. It should be noted that similar studies by Mazouffre et al. show largely differing effects on temperature when the anode power is altered by discharge voltage than when it is altered by propellant mass flow rate.[12]

Further validation of the infrared data with a thruster heating model, the coupling of thermal with performance data, and a comparison of camera calibration techniques are works for future study. Further examination of the correlation between insulator temperature and erosion is also suggested.

American Institute of Aeronautics and Astronautics

References

[1] Zinc selenide optics. http://www.laseroptex.com/PROznsewindows.asp, 2005.

[2] A. Anikin, S. Bednov, A. Golikov, and M. Yasinsky. Thermovision study of temperature fields and radiation characteristics of electric thruster t-100 surfaces. In *24th IEPC*, Moscow, Russia, September 1995.

[3] B. Archipov, L. Krochack, and N. Maslennikov. Thermal design of the electric propulsion system components: Numerical analysis and testing at fakel. *AIAA*, 1998.

[4] L. Cassady and E. Choueiri. High accuracy multi-color pyrometry for high temperature surfaces. In *28th IEPC*, Toulouse, France, 2003.

[5] A. Coutrot, J. Bugeat, M. Lyszyk, and D. Valentian. Spt m 2 development status. In *31st Joint Propulsion Conference*, San Diego, CA, July 1995.

[6] M. Domonkos, A. Gallimore, and M. Patterson. Thermographic investigation of 3.2 mm diameter orificed hollow cathodes. *AIAA*, 1998.

[7] S. Roche et al. Thermal analysis of a stationary plasma thruster. In *35th Joint Propulsion Conference*. AIAA-1999-2296, June 1999.

[8] D. Jacobsen, D. Manzella, R. Hofer, and P. Peterson. Nasa's 2004 hall thruster program. In *40th Joint Propulsion Conference*, Ft Lauderdale, FL, July 2004.

[9] R. Jankovsky, C. McLean, and J. McVey. Preliminary evaluation of a 10kw hall thruster. In *37th AIAA Aerospace Sciences Meeting and Exhibit*, Reno, NV, January 1999.

[10] W.A. Hargus Jr. and G. Reed. The air force clustered hall thruster program. In *38th Joint Propulsion Conference*. AIAA-2002-3678, July 2002.

[11] D. Massey, L. King, and J. Makela. Progress on the development of a direct evaporation bismuth hall thruster. In *41st Joint Propulsion Conference*, Tucson, AZ, July 2005.

[12] S. Mazouffre, P. Echegut, and M. Dudeck. A calibrated infrared imaging study on the steady state thermal behaviour of hall effect thrusters. *Institute of Physics Publishing*, 2007.

[13] A.N. Raneev, A.A. Semenov, and O.B. Sololyev. Surface temperature influence onto ceramic sputtering rate. In *XIII International Conference about ion interaction with a surface*, Moscow, 1997.

[14] T. Sarvery-Verhey. 28,000 hour xenon hollow cathode life test results. In *25th IEPC*, Cleveland, OH, August 1997.

[15] R. Siegel and J. Howell. *Thermal Radiation Heat Transfer*. Hemisphere Publishing Corporation, second edition, 1981.

[16] B. Zhang, J. Redgrove, and J. Clark. A transient method for total emissivity determination. *International Journal of Thermophysics*, 2004.